

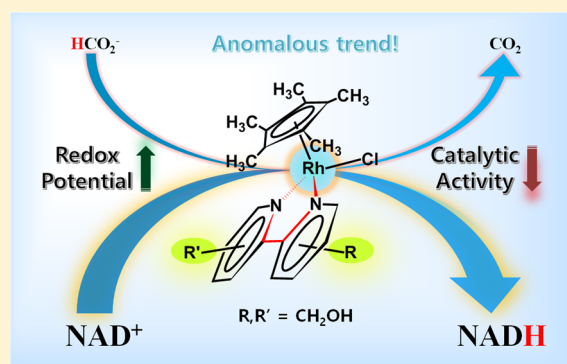
Correlation between the Structure and Catalytic Activity of [Cp*Rh(Substituted Bipyridine)] Complexes for NADH Regeneration

Vinothkumar Ganesan, Dharmalingam Sivanesan, and Sungho Yoon*

Department of Bio & Nano Chemistry, College of Natural Sciences, Kookmin University, 861-1 Jeoungnung-dong, Seongbuk-gu, Seoul 136-702, Republic of Korea

Supporting Information

ABSTRACT: A series of water-soluble half-sandwich [Cp*Rh^{III}(N[^]N)Cl]⁺ (Cp* = pentamethylcyclopentadiene, N[^]N = substituted 2,2'-bipyridine) complexes containing electron-donating substituents around the 2,2'-bipyridyl ligand were synthesized and fully characterized for the regioselective reduction of nicotinamide coenzyme (NAD⁺). The influence of the positional effect of the substituents on the structural, electrochemical, and catalytic properties of the catalyst was systematically studied in detail. The catalytic efficiency of the substituted bipyridine Cp*Rh^{III} complexes are inversely correlated with their redox potentials. The 5,5'-substituted bipyridine Cp*Rh^{III} complex, which had the lowest reduction potential, most effectively regenerated NADH with a turnover frequency of 1100 h⁻¹. Detailed kinetic studies on the generation of intermediate(s) provide valuable mechanistic insight into this catalytic cycle and help to direct the future design strategy of corresponding catalysts.

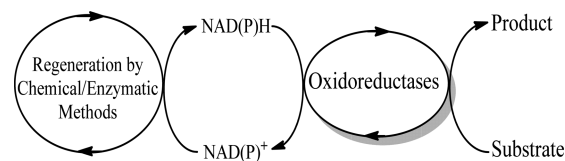


1. INTRODUCTION

Biotransformations are evolving as key industrial processes for the production of fine chemicals, especially in the pharmaceutical industry, where chemo-, enantio-, and regioselective syntheses are very critical.¹ It has been predicted that by 2050 biocatalysis and bioconversions may account for more than 30% of industrial production.^{2,3} Among the enzymes used in biotransformations, oxidoreductase is involved in a diverse range of applications; currently many commercially applied processes involve oxidoreductases.^{4–6} In this context, oxidoreductase-mediated asymmetric biotransformations are of significant importance because they are utilized in the synthesis of amino acids, chiral compounds, steroids, and other pharmaceutically important entities. Furthermore, applications of oxidoreductases can also be seen in diverse areas such as biomass transformation, polymer synthesis, environmental protection, the food industry, organic synthesis, oxidation of hydrocarbons, and biosensors.^{7,8} Nevertheless, oxidoreductases mostly operate in tandem with nicotinamide coenzymes (NADH) or its phosphorylated form (NAD(P)H; Scheme 1), which limits its commercial applicability given the high cost, stoichiometric usage, and physical instability of NAD(P)H. If a suitable NAD(P)H regeneration system is developed, it may lead to an easy route for biocatalysis, which may replace the complicated, hazardous, and expensive chemical catalytic route of many industrial intermediates and chemicals.⁹

In terms of the regeneration of a coenzyme, there are two major catalytic regeneration methods available: enzymatic regeneration and nonenzymatic regeneration.¹⁰ Although the

Scheme 1. Schematic Diagram for Oxidoreductase Usage in Biotransformations in Tandem with NAD(P)H



enzymatic method is promising because of its mild conditions and high total turnover number (TTN), its disadvantages, such as high enzyme cost, enzyme instability, requirement of buffers to maintain the pH, and costly downstream processes for product separation fuel the need for other regeneration approaches.^{10–12} Conversely, nonenzymatic approaches, i.e., the chemical, electrochemical (direct and indirect), and photochemical methodologies, suffer from a low TTN, a low product selectivity, a deleterious NAD₂ dimer formation, and the requirement for a sacrificial electron donor, mediator, photosensitizer, etc.^{10–13} Despite the fact that the chemical regeneration method has these limitations, the rapid development of organometallic chemistry offers strategies for designing catalysts with high activity and specificity, along with the usage of dihydrogen or formate as a cheap hydride source. Many chemical regeneration catalysts consisting of organometallic complexes have been reported using ruthenium, rhodium, and

Received: October 11, 2016

iridium metals.^{14–25} Of these, rhodium complexes are of particular importance owing to their high activity, 1,4-regioselectivity, and high stability across a wide range of experimental conditions.^{17–23} The cationic pentamethylcyclopentadienyl (Cp*) rhodium bipyridine complex $[\text{Cp}^*\text{Rh}(\text{bpy})\text{Cl}]^+$ is the most widely used catalyst owing to its versatile range of applications and its chemical and electrochemical regeneration flexibility and regiospecific activity.^{17–21} Notwithstanding the foregoing, the system also suffers from low TTN, which leads to the use of a large amount of catalyst compared to the amount of enzymes in the biotransformation system. Consequently, poor stability and mutual inactivation of the catalyst and enzymes are major drawbacks when chemical regeneration is combined with reductase enzymes.^{26–28} Therefore, a highly active catalyst could reduce the deleterious interaction between the catalyst and enzyme by minimal usage of organometallic catalysts.

Previous experimental evidence suggests that the catalytic activity is mainly dependent on the electron density of the central metal cation, which is a result of the nature of the substituents on the bipyridine (bpy) ring.^{17,19,20} It is also believed that the catalytic efficiency of catalysts can be tuned based on both the kind and position of the substituents in the bpy ligands. Although there have been scattered reports on how the different functional groups influence the properties of the ligands and complexes for NAD(P)H regeneration, a detailed systematic study is not yet available.^{17,19–21} To design a catalyst with high activity and selectivity, it is necessary to understand how the structure and functional groups influence the activity of the catalytic systems of NAD(P)H regeneration.

As our first attempt in this direction, we have designed catalysts with electron-donating substituents around the bpy ligand. Herein, we report on a series of water-soluble rhodium complexes with hydroxymethyl functional groups at different positions of the bpy ring that can catalyze NAD(P)H regeneration with various activities. Results of the structure, redox behavior, and activity of the catalysts, together with kinetic studies provide valuable insight into the unprecedented relationship between the structure and activity of the synthesized rhodium catalysts for NADH regeneration.

2. EXPERIMENTAL SECTION

2.1. General Procedure and Physical Measurements. All chemicals purchased were of analytical grade from Sigma-Aldrich Chemical Co. and were used without further purification unless mentioned otherwise. The rhodium dimer $\{(\eta^5\text{-Cp}^*)\text{Rh}(\mu\text{-Cl})\text{Cl}\}_2$ was prepared using a reported procedure.²⁹ UV–vis spectra were recorded using a SCINCO S-3100 spectrophotometer with a photodiode array (PDA) detector. ¹H and ¹³C NMR spectra were recorded on Bruker 400 MHz and Bruker 125 MHz instruments, respectively.

2.2. Cyclic Voltammetry. Cyclic voltammetry studies were carried out using a ZAHNER-elektrok IM6 potentiostat. The cell was a standard three-electrode system with a platinum wire as the counter electrode, a glassy carbon or platinum electrode as the working electrode, and Ag/AgCl as the reference electrode. Tris-(hydroxymethyl)aminomethane (Tris)/HCl (0.100 M, pH 7.5) was used as an electrolyte. The electrochemical system was calibrated with 2.03 mM $\text{K}_3\text{Fe}(\text{CN})_6$.

2.3. Single-Crystal X-ray Structural Analysis. A single crystal was mounted at room temperature on the tips of quartz fibers, coated with Paratone-N oil, and cooled under a stream of cold nitrogen. Intensity data were collected on a Bruker CCD area diffractometer running the SMART software package, with Mo K α radiation ($\lambda = 0.71073 \text{ \AA}$). The structure was solved by direct methods and refined

on F^2 using the SHELXTL software package.³⁰ Multiscan absorption correction was applied with SADABS,³¹ part of the SHELXTL program package. The structure was checked for higher symmetry by the program PLATON.³² All non-hydrogen atoms were refined anisotropically. In general, hydrogen atoms were assigned idealized positions and given thermal parameters equivalent to 1.5 times (methyl hydrogen atoms) and 1.2 times (all other hydrogen atoms) the thermal parameter of the carbon atom to which they were attached. Complex 2 has a disorder due to the steric hindrance of the substituents. Complex 5 contains one methanol molecule in the crystal lattice.

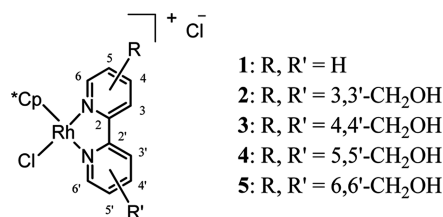
2.4. Kinetic Measurements. The kinetic experiments were carried out in a SCINCO S-3100 UV–vis spectrophotometer with a PDA detector, attached to a Peltier temperature controller. A stock solution of catalysts (1.14 mM, 2.00 mL) and sodium formate (0.350 M) was made for kinetic experiments in an argon-saturated phosphate buffer (pH 7.2). A solution of NAD⁺ ($1.05 \times 10^{-4} \text{ M}$) in a sodium formate stock solution was made in a volumetric flask. A 2.42 mL aliquot of this solution was transferred to a thermostated airtight quartz UV–vis cell of 1 cm path length using a micropipette and purged with argon for 5 min. The sample was then brought to $27 \pm 0.1 \text{ }^\circ\text{C}$ in the UV–vis spectrometer temperature controller before the required volume of a catalyst stock solution (77.0 μL , 17.5 μM in 2.50 mL) was added via an argon-purged syringe under argon positive pressure and mixed quickly. The absorbance increase was monitored until all of the starting material was converted.

2.5. Catalytic NADH Regeneration. The catalytic conversion of NAD⁺ to NADH by catalysts 1–5 (3.50 μM) was carried out in a phosphate buffer (5.00 mL) of pH 7.2 containing sodium formate (HCO_2Na ; 0.350 M) as a reducing agent and NAD⁺ (3.50 mM) at 60 $^\circ\text{C}$. The conversion was determined by the UV–vis absorption of generated NADH at 340 nm. Turnover frequencies (TOFs) were calculated from the conversion observed after 30 min of catalytic reaction.^{17,19,20}

3. RESULTS AND DISCUSSION

3.1. Preparation and Structural Characterization of the Complexes. To understand how the positions of the substituents influence the structure, redox behavior, and catalytic activity of the complexes for the NAD(P)H cofactor regeneration, systematic variation of the bpy ligand with the $-\text{CH}_2\text{OH}$ substitutional group was performed (Chart 1). To

Chart 1. Structure of $[\text{Cp}^*\text{Rh}^{\text{III}}(\text{N}^{\wedge}\text{N})\text{Cl}]\text{Cl}$ Complexes



synthesize complexes 2–5, the dihydroxymethyl-substituted 2,2'-bpy ligands were synthesized according to a literature procedure.³³ This was followed by reaction with $[\text{Cp}^*\text{Rh}(\mu\text{-Cl})\text{Cl}]_2$ to yield the corresponding water-soluble yellowish-orange cationic complexes in excellent yield (detailed synthetic procedures are shown in the Supporting Information). Air-stable reddish-orange crystals of complexes 2 and 5 that were suitable for X-ray diffraction were obtained in a methanol/diethyl ether system by the vapor diffusion method. The crystal structures of complexes 2 and 5 are shown in Figure 1, and the selected bond distances and bond angles are given in Table S1. The crystallographic data of complexes 1 ($[\text{Cp}^*\text{Rh}(\text{bpy})\text{Cl}]\text{Cl}$) and 3 ($[\text{Cp}^*\text{Rh}(4,4'\text{-CH}_2\text{OH-bpy})\text{Cl}]\text{Cl}$) were previously

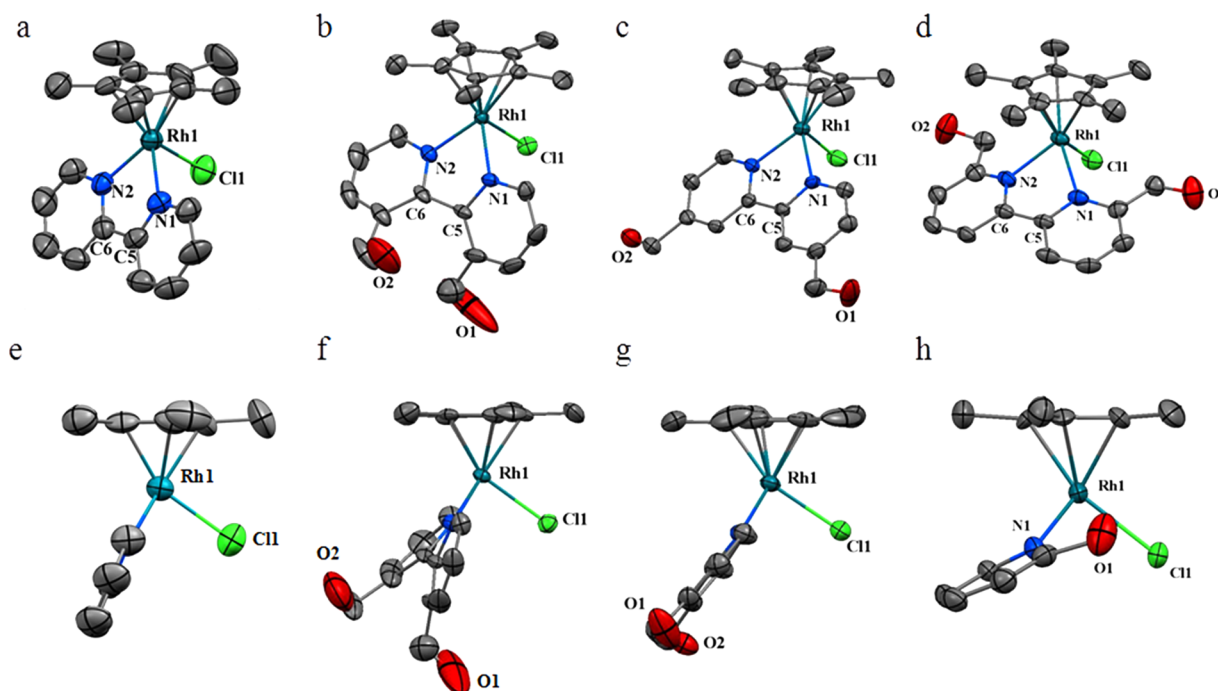


Figure 1. ORTEP diagrams of complexes (a) **1**,³⁴ (b) **2**, (c) **3**,²⁰ and (d) **5** showing 50% probability of the thermal ellipsoids. (e–h) Side views of the catalysts in the same order. Hydrogen atoms and counteranions are omitted for clarity.

reported,^{34,35,20} and the crystallization of complex **4** was not successful despite repeated attempts.

The structures of complexes **2** and **5** contain a rhodium(III) center with piano-stool-like half-sandwich geometry that is surrounded by a Cp* ring, a substituted bpy, and one anionic chloride ligand. Rhodium(III), being bound to the Cp* anion in an η^5 fashion, two nitrogen atoms of the substituted bpy, and one chloride anion, generates a monocationic $[(\eta^5\text{-Cp}^*)\text{-Rh}^{\text{III}}(\text{CH}_2\text{OH-bpy})(\text{Cl})]^+$ species. One chloride counteranion is located in the crystal lattice to balance the charge neutrality, which confirms that the rhodium is in the 3+ formal oxidation state. It is worth noting that the two pyridine rings in complexes **2** and **5** are not in one plane, which is different from the configuration of the rings in complexes **1** and **3** (which are in one plane). This may originate from the steric hindrance posed by two adjacent bulk substituent groups ($-\text{CH}_2\text{OH}$).

In complex **2**, the bond distances between Rh1 and the coordinated N1 and N2 of the substituted bpy are 2.114(5) and 2.103(5) Å, respectively. The Rh1–N1 bond is longer than the reported value of 2.100(5) Å for complex **1**.^{34,35} Similarly, in complex **5**, the Rh1–N1 and Rh1–N2 bonds have a distance of 2.126(5) Å, which is longer than the reported values for complexes **1** and **3**.^{20,34,35} The observed elongation of the Rh1–N bond may originate from the twisted bpy ring configurations by substitution at the 3,3' or 6,6' positions, resulting in a different electronic effect in the formation of coordination bonds between rhodium and the chelating bpy ligand.

The biting angles within N1–Rh1–N2 for complexes **2** and **5** are 77.1° and 76.7°, respectively, which are higher than the reported value of 75.3° for complex **1**.^{34,35} The bond distances between the rhodium cation and anionic chloride ligand are 2.397(2) and 2.387(2) Å for complexes **2** and **5**, respectively. This is relatively long compared with the reported Rh–Cl bond length of 2.363(3) Å for complex **3**, indicating their ease of

ionization in an aqueous medium to readily form the dicationic rhodium aqua complex.

3.2. Catalysts in Solution. The patterns of the electronic spectra of complexes **2**–**5**, depicted in Figure S1 (selected information in Table S3), are similar to that of **1**, indicating that the rhodium(III) metal center in complexes **2**–**5** has distorted octahedral geometry similar to that of **1**. The electronic spectra of **2**–**5** show strong UV–vis absorption bands at 230–236 nm for ligand-centered transitions. The absorption maxima observed in the range 309–327 nm can be assigned to metal-to-bpy ligand charge-transfer (MLCT) transitions, and the broad shoulder bands observed around 350–400 nm may be attributed to ligand-to-metal charge-transfer (LMCT) [$\pi(\text{Cp}^*)\text{-to-d}(\text{Rh}^{\text{III}})$] bands.^{36–38}

To understand the configuration of complexes **2** and **5** in solution, which may differ from that in the solid state, ¹H NMR spectra were measured for the complexes. The ¹H NMR spectra of the complexes are shown in Figures S2–S5 and Table S4. The downfield shift of ligand protons upon coordination indicates the shift of the electron density toward the cationic rhodium(III) metal center after coordination. The Cp* protons of complex **5** resonate upfield at 1.48 ppm; this can be compared with complex **2**, which resonates at 1.6 ppm, and complexes **3** and **4**, which both have the Cp* peak at ~1.7 ppm. The upfield shift of the Cp* peaks on complexes **2** and **5** indicates that more electron density is localized on the anionic Cp* ring of these complexes compared with complexes **3** and **4**. This confirms that the long bond distance between the Cp* ring and rhodium metal center found in the crystal structure of complexes **2** and **5**. It may originate from the steric effect of the substituents in the bpy ligand.

3.3. Electrochemical Properties of Catalysts. To evaluate the electronic effect of the substituent's position on the metal center, the redox behavior of complexes **2**–**5** was studied by cyclic voltammetry in aqueous solutions containing Tris/HCl as a supporting electrolyte (0.100 M Tris/HCl of pH

7.5). The redox potentials of the complexes are listed in Table 1, and the cyclic voltammograms are shown in Figures S6 and

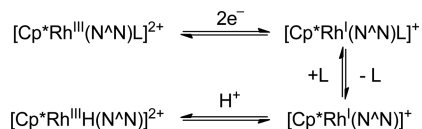
Table 1. Summary of the Redox Potential and NADH Regeneration Activity of Catalysts 1–5

catalyst	redox potential of complex vs Ag/AgCl (mV)	hydride generation rate constant ^b k_1 (10^{-3} s^{-1})	activity ^b (TOF h^{-1})
1	−760	6.41	875 ^c
2	−960	3.29	120 ± 2
3	−770	6.76	710 ^d
4	−730	7.04	1100 ± 20
5	−900	3.35	100 ± 2

^aReaction conditions: 35.0 μM catalyst, 0.35 M HCO_2Na in a degassed phosphate buffer of pH 7.2. ^bRegeneration of NADH (chemical method): NAD^+ -to-catalyst ratio = 1000 using 0.350 M HCOONa in a phosphate buffer (pH 7.2) at 60 °C. TOF was calculated based on the UV–vis absorbance of NADH at 340 nm. ^cReference 19. ^dReference 20.

S7. Because these redox mediator complexes readily form water-ligated complexes in aqueous solutions, the redox-active form may be the $[\eta^5\text{-Cp}^*\text{Rh}(\text{CH}_2\text{OH-bpy})(\text{H}_2\text{O})]^{2+}$ species. All of the complexes showed irreversible double-reduction peaks (Rh^{III} to Rh^{I}) in the range of −0.730 to −0.960 mV versus Ag/AgCl at a scan rate of 100 mV s^{-1} . Complexes 2 and 5 had the highest reduction potentials (−0.960 and −0.900 mV, respectively) among all of the complexes as a result of the electron-donating substituents at the 3,3' and 6,6' positions, respectively. The 4,4'-substituted complex 3 had a reduction potential of −0.770 mV, as reported.²⁰ Complex 4 had a reduction potential of −0.730 mV, as the 5,5' substitution could only increase the bpy basicity, rather than the electron density on the metal center.¹⁹ The reduction process and irreversible character of the reduction peak are explained by the following mechanism (Scheme 2). As reported previously, the short-lived

Scheme 2. Electrochemical Reduction of the Metal Complexes in a Tris/HCl Buffer of pH 7.5 ($\text{Cp}^* = \text{Pentamethylcyclopentadiene}$ and $\text{N}^*\text{N} = \text{substituted } 2,2'\text{-bpy}$; $\text{L} = \text{H}_2\text{O}$)



reduced form of the complex $[\eta^5\text{-Cp}^*\text{Rh}^{\text{I}}(\text{CH}_2\text{OH-bpy})(\text{H}_2\text{O})]$ takes up a proton in its ligand sphere, forming the corresponding hydride complex $[\eta^5\text{-Cp}^*\text{Rh}^{\text{I}}(\text{CH}_2\text{OH-bpy})(\text{H})]^+$ of the rhodium(III) cation.¹⁷ Therefore, the reduced rhodium(I) complex is no longer available for a reverse potential sweep to become oxidized. As revealed by the redox potential, the electron-donating CH_2OH substituent present at the 3,3' and 6,6' positions strongly increases the electron density at the metal center for complexes 2 and 5, and it has less effect if the substitution is at the 4,4' position in complex 3. Conversely, in comparison to complex 1, the redox potential was positively shifted in the 5,5'-substituted complex 4.

3.4. Rates of Intermediate (Metal Hydride) Generation. Because regeneration of the cofactor $[\text{NAD(P)H}]$ is dependent on the rate of metal hydride generation, the kinetics of metal hydride generation using catalysts 2–5 were studied in

detail using HCO_2Na as a hydride source,^{39,40} in the aqueous phosphate buffer solution at pH 7.2. (see the Supporting Information, p S17, for the detailed procedure). Interestingly, the reaction progress was clearly seen with an absorbance increment in the UV region, and discernible, but rather broad, absorption bands were observed in the visible regions. A set of three isosbestic points observed in the series of kinetic UV–vis spectra indicates the quantitative conversion of $[\eta^5\text{-Cp}^*\text{Rh}(\text{CH}_2\text{OH-bpy})(\text{H}_2\text{O})]^{2+}$ to a single species. The reaction was studied with the absorbance versus time plot at a wavelength of 287 nm for complexes 2 and 5, 286 nm for complex 4, and 281 nm for complex 3, which was attributed to the intermediate species of the corresponding parent complexes.^{36–38,40–42}

Figure 2 shows the UV–vis spectral changes during the

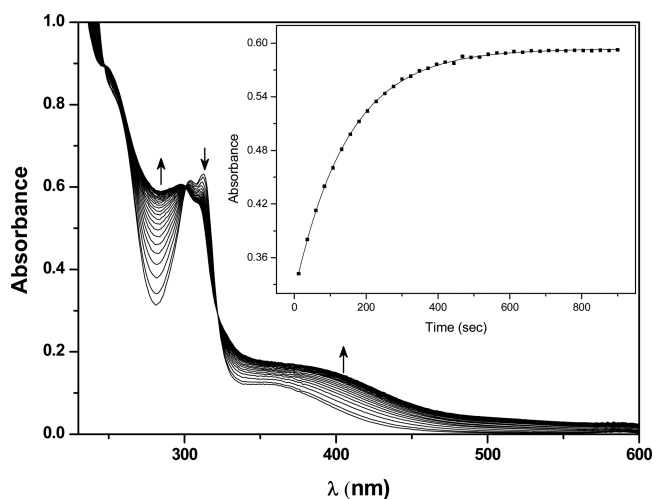


Figure 2. UV–vis kinetic traces of catalyst 3 in a reaction with HCO_2Na . Inset: Exponential curve fitting of the absorbance (at 281 nm) versus time plot.

reaction of complex 3 with HCO_2Na (see Figures S8–S11 for complexes 1, 2, 4, and 5, respectively). The absorption growth curve was fitted with a pseudo-first-order kinetic equation versus the concentration of the catalysts, and the rate constants (k_{obs}) were determined. The observed rate constants are shown in Table 1 and follow the order $4 > 3 \gg 5 \approx 2$. It is worth noting that catalysts with lower redox potential generate the intermediate faster than catalysts with higher redox potential (inverse trend). However, the hydride generation activity trend is contrary to the previously observed trend, where the increased electron density on the rhodium center led to increased activity.^{17,19–21}

3.5. Electrochemical Regeneration of NADH. The conversion of NAD^+ to NADH by direct and indirect electrochemical methods has been studied; the direct electrochemical reduction of NAD^+ requires high overpotential; meanwhile, the indirect one requires an elaborated redox mediator, such as ferredoxin- NAD^+ reductase⁴³ or the cationic (bipyridine)rhodium complex.¹⁷ To test that the complexes 3–5 could indirectly mediate electrochemical NADH regeneration, electrochemical studies of the equimolar concentrations of NAD^+ and the corresponding compounds were performed, resulting in reduction peaks at −814, −985, and −915 mV, respectively [Figure 3 (dotted lines)]; because deleterious dimeric NADH inactivation by direct electron transfer occurs at −942 mV versus Ag/AgCl through the first reduction of NAD^+ ,⁴⁴ indirect electrochemical generation of NADH was not

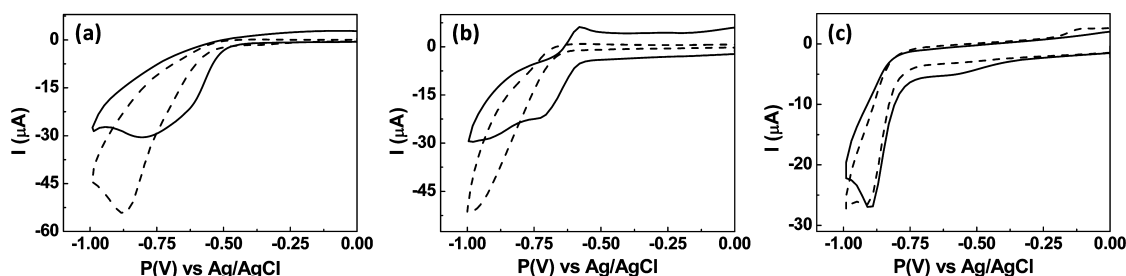


Figure 3. Cyclic voltammograms of complexes 3 (a), 4 (b), and 5 (c) (solid lines) with NAD^+ (dotted lines).

performed with complex **2**, which has a redox potential at -960 mV. The reduction current that was produced from these systems was much higher than that from the corresponding complex alone. It indicated the combined reduction of rhodium(III)/rhodium(I) and the fast reduction of NAD^+ to NADH by rhodium(I) species regenerating rhodium(III) species, which demonstrates the successful mediation of indirect electrochemical regeneration of NADH by compounds **3–5**. It is worth noting that these compounds with hydroxyl end groups (potential anchoring groups) can be attached to the electrode to ensure the long-term stability of the system.

3.6. Chemical Regeneration of NADH . Many synthetic applications of enzymatic reactions are restricted by their dependence on NADH or its NAD(P)H as cofactors. Steckhan and Fish et al. introduced $[\eta^5\text{-Cp}^*\text{Rh}(\text{bpy})(\text{H}_2\text{O})]^{2+}$ as a catalyst for NAD(P)H regeneration and studied it extensively.^{17,18,39,45,46} To determine the influence of a substituent's position on the catalytic activity for the regioselective reduction of NAD^+ with formate anions as a sacrificial hydride source in a phosphate buffer solution, the catalytic activity of complexes **2–5** was studied under the same conditions as those of catalyst **1**. The regeneration of NADH was monitored and quantified by the increase in the absorbance peak at 340 nm using UV–vis spectrometry. Catalysts **2–5** were effective at promoting the regeneration of NADH in a phosphate buffer solution of pH 7.2 . To check the maximum TOF, the substrate-to-catalyst ratio was maintained at 1000 and the temperature was maintained at 60 °C. The results obtained are shown in Table 1. The best catalytic activity was obtained with complexes **3** and **4**, with TOFs of 710 and 1100 h^{-1} , respectively. In comparison with catalyst **1** (875 h^{-1} ; the commonly used catalyst for cofactor regeneration), catalyst **4** showed the best TOF value, and the catalyst **3** TOF value was close to that of complex **1**.¹⁹ However, complexes **2** and **5** have very low TOFs of 120 and 100 h^{-1} , respectively. As reported, this NADH regeneration activity trend is proportional to the rhodium hydride species generation trend, as shown in Table 1.

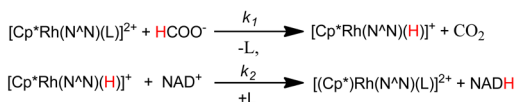
3.7. Effect of the Catalyst Structure on the NADH Regeneration Activity. The coordination geometry of complexes **2** and **5** is different from that of unsubstituted bpy complex **1** and $4,4'$ -substituted bpy complex **3**. Interestingly, as shown in Figure 1, the Rh1, N1, C1, C6, and N2 atoms of the five-membered rhodacycle of complexes **2** and **5** do not lie in one plane and give the rhodacycle a puckered shape, although the same atoms of complexes **1** and **3** lie in almost the same plane.^{20,34,35} The shape of the rhodacycle is like an open mail envelope for complex **5**, whereas it is a twisted paddle shape for complex **2**. This unusual coordination mode of complexes **2** and **5** is caused by the steric congestion of the ligand, as depicted by the space-filling model of the crystal structure (Figure S13). In complex **2**, the intrinsic steric repulsion

between two adjacent hydroxymethyl groups (gauche-type effect) twists the pyridine rings of the bpy ligand into a twisted paddle shape. Conversely, the steric repulsion between the Cp^* ring and hydroxymethyl groups puckers the rhodacycle of complex **5**. In complex **5**, the elongated bond distance (from 2.100 to 2.126 Å) between the rhodium metal and nitrogen atoms of the bpy ring is the evidence of the consequence of this steric effect. A similar unusual coordination mode (as a consequence of the sterical behavior of $6,6'$ -substituted bpy complexes) was also observed by Fukuzumi et al.^{49,50} As a result of this unusual metallacycle shape, the bond distances between the rhodium center and carbon atoms of the Cp^* ring are elongated for complexes **2** and **5** (in comparison with complexes **1** and **3**; Table S1). The dihedral angle between the planes of two pyridine rings of complex **2** is 31.6° , whereas in complex **5**, the dihedral angle formed between the planes of N1–C5–C6–N2 and Rh1–N1–N2 is 154.5° . The same dihedral angle for the already reported complexes **1** and **2**, and for complex **3**, is close to 172 – 177° ($\sim 180^\circ$, almost in a plane). This unusual coordination mode, and the dihedral angle change induced by the sterical effects of the ligands, plays a role in the low catalytic activity of complexes **2** and **5**. Previous studies¹⁷ also explain the low catalytic activity of $[\text{Cp}^*\text{Rh}(6,6'\text{-CH}_3\text{-bpy})(\text{Cl})]^+$ due to its sterical interference of methyl groups with formate ions to slow down rhodium hydride formation. The higher dihedral angle change caused by the weird metallacycle also has an important role that cannot be ignored. Hence, complex **2** does not have any sterical influence around the metal center; rather, it has only a puckered metallacycle with low catalytic efficiency similar to that of complex **5**.

3.8. Regeneration Mechanism. To unravel how a substituent's position affects the rate-determining step of the regeneration mechanism, it is important to understand the reaction pathways and regeneration mechanism in detail. In the past, all cofactor regeneration methods that involved an organometallic mediator strongly indicated that the regeneration proceeds through the metal hydride intermediate ($[\text{Cp}^*\text{Rh}(\text{N}^{\wedge}\text{N})(\text{H})]^+$), which was reported as the rate-determining step of the overall reaction (Scheme 3, Route-A).^{17–21,24,25} However, recently there were two reports that stated that the intermediate obtained for catalyst **1**, $[\text{Cp}^*\text{Rh}(\text{bpy})\text{Cl}]^+$, is not a $\text{Rh}-\text{H}$ species but rather formed from reductive elimination of the proposed rhodium hydride and bears $[\eta^4\text{-Cp}^*\text{-H}]$ as the active hydride-transfer species ($[(\eta^4\text{-Cp}^*\text{-H})\text{Rh}(\text{N}^{\wedge}\text{N})]^+$; Scheme 3, Route-B).^{41,42} As evidenced from the rate constant (k_1) values of hydride intermediate generation and the TOF values in Table 1, the catalytic order is $4 > 3 \gg 5 \approx 2$, and it is clear that the activity is in direct relation with intermediate generation and is greatly affected by the substituent's position. Among catalysts **2–5**, catalysts **2** and

Scheme 3. Proposed Kinetic Routes for NADH Regeneration by $[\text{Cp}^*\text{Rh}^{\text{III}}(\text{N}^{\wedge}\text{N})\text{L}]^+$ Catalyst Involving Both Rhodium Hydride (Route-A) and a $\text{Cp}^*\text{-H}$ Intermediate (Route-B)^a

Route-A



Route-B



^a Cp^* = pentamethylcyclopentadiene, $\text{N}^{\wedge}\text{N}$ = (2,2'-bpy); L = H_2O .

5 have shown much less activity; this is due to their slower intermediate generation step, as shown by their k_1 values. The UV-vis kinetic traces of catalysts 1–4 are similar in the visible region (Figures S8–S11), however, the UV-vis kinetic traces of catalyst 5 (which are dissimilar to catalysts 2–4 in the visible region; Figures S8–S12) suggest that 5 can have a different intermediate species in comparison with catalysts 2–4. To gain some insight about the formed intermediate species, complexes 2–5 were treated with HCO_2Na in D_2O at room temperature (Figure 4). ^1H NMR spectra of the resultant intermediate species from complexes 2–4 did not show any peaks in the negative region; however, the Cp^* peak was partially split into four peaks with a ratio of 6:6:3:1, which suggests that catalysts 2–4 could have $[(\eta^4\text{-Cp}^*\text{-H})\text{Rh}(\text{N}^{\wedge}\text{N})]^+$ as an intermediate species similar to that of catalyst 1 (indicated as asterisks in Figure 4a–c). Conversely, observation of the typical Rh–H

peak at -7.21 ppm in the ^1H NMR spectra of complex 5 with a formate salt confirms that it does not undergo a reductive elimination reaction (k'_1) to generate the $[(\eta^4\text{-Cp}^*\text{-H})\text{Rh}(\text{N}^{\wedge}\text{N})]^+$ species. The elongated bond distance between the rhodium metal and Cp^* carbon atoms of 5, caused by the steric effect of the substituent, could be the reason for the absence of the k'_1 step in the catalytic process. Therefore, catalyst 5 could be seen to reduce NAD^+ through the $[\text{Cp}^*\text{Rh}(\text{N}^{\wedge}\text{N})(\text{H})]^+$ intermediate.

On the basis of our observed experimental results and earlier reports,^{17–23,39,45–48} we postulate a plausible mechanism (Scheme 4) for the regeneration of NAD(P)H in aqueous solution using catalysts 2–5. In an aqueous medium, the cationic rhodium complex readily formed the water-coordinated aqua complex $[\eta^5\text{-Cp}^*\text{Rh}(\text{N}^{\wedge}\text{N})(\text{H}_2\text{O})]^{2+}$, which reacts with the formate anion (HCOO^-) via β -hydride elimination to produce CO_2 and the intermediate rhodium hydride complex $[\eta^5\text{-Cp}^*\text{Rh}(\text{N}^{\wedge}\text{N})(\text{H})]^+$. Then, catalysts 2–4 follow Route-B, where the subsequent reductive elimination produces the $[(\eta^4\text{-Cp}^*\text{-H})\text{Rh}(\text{N}^{\wedge}\text{N})]^+$ intermediate complex. NAD^+ is coordinated through amide functionality, and the endo orientation of the C–H bond ideally transfers the hydride while maintaining 1,4 regioselectivity.⁴¹ In Route-A, which involves only catalyst 5, NAD^+ is coordinated to the $[\eta^5\text{-Cp}^*\text{Rh}(\text{N}^{\wedge}\text{N})(\text{H})]^+$ complex through amide functionality, and the hydride is concertedly transferred via a kinetically favored six-membered transition state to give the 1,4-regioselective product. Finally, in both pathways, the water molecule displaces the 1,4-dihydro product to complete the catalytic cycle.

All of the studies previously reported using (substituted bpy) $\text{Cp}^*\text{-Rh}$ complexes showed a direct relationship between the redox potential and rhodium hydride generation, the NAD(P)H regeneration activity. However, our detailed study

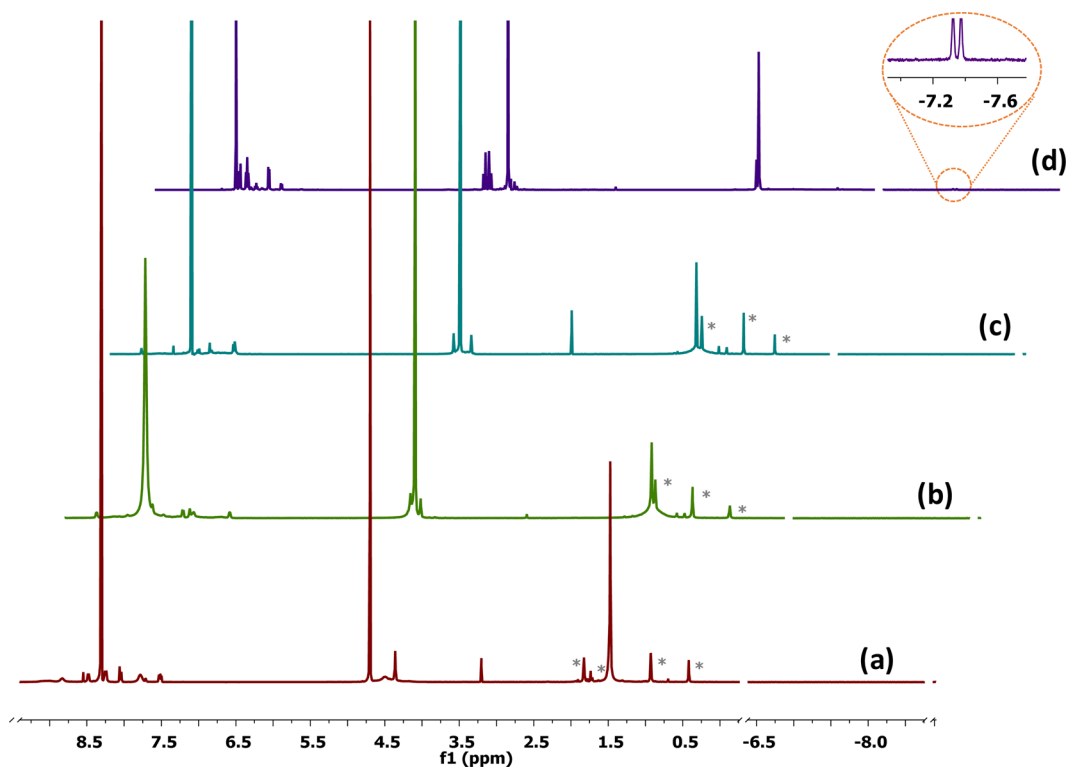
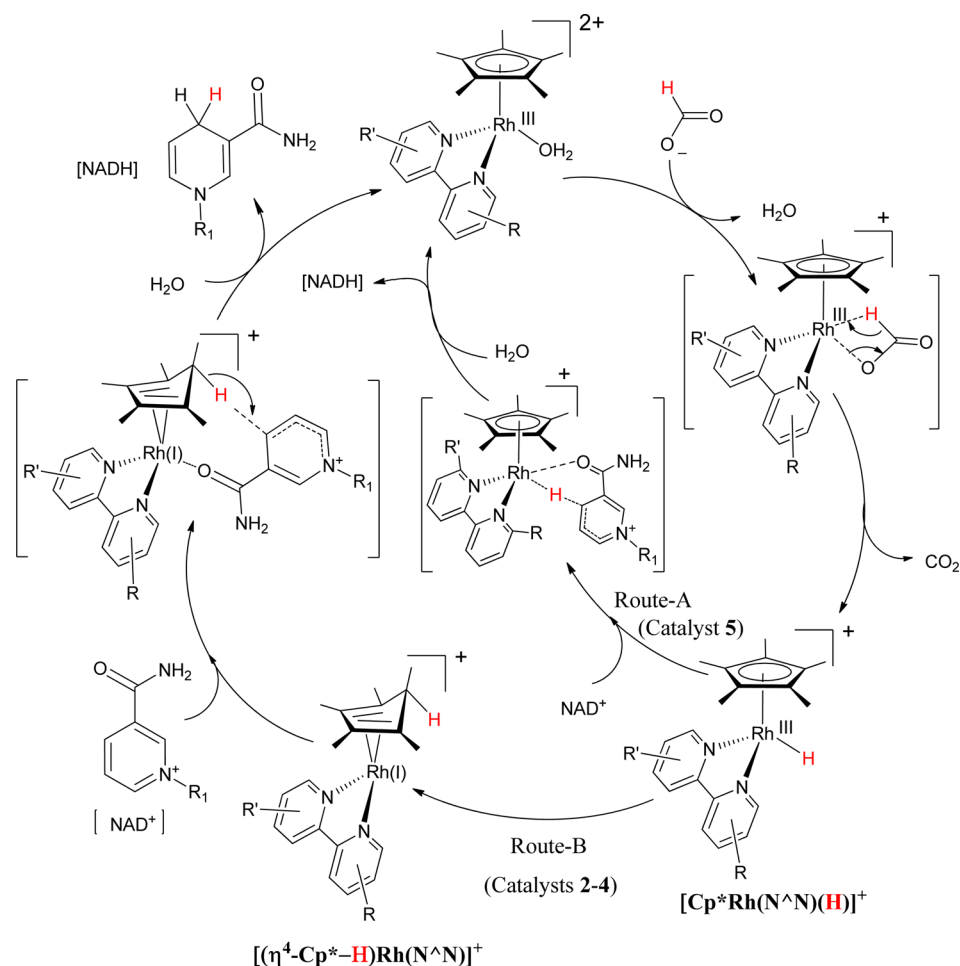


Figure 4. ^1H NMR spectra of generated intermediates upon the treatment of complexes 2 (a), 3 (b), 4 (c), and 5 (d) with HCO_2Na , respectively. (Full spectra of complexes 2–5 are given in Figures S14–S17.)

Scheme 4. Plausible Mechanism for the Regeneration of NADH Using Catalysts 2–5



on the positional effect of the substituents in the bpy ring shows an inverse relationship between the redox potential and intermediate generation. Sterical implications of the substituent's position restrict the rate of intermediate generation even though the metal center has a higher redox potential. Moreover, our studies show that the position of the substituent is very important in deciding the catalyst structure, redox potential, and activity for the regeneration of NADH.

4. CONCLUSION

In conclusion, we have synthesized hydroxymethyl-substituted half-sandwich rhodium(III) complexes for NADH regeneration. Spectroscopic, crystallographic, electrochemical, and kinetic studies showed how the positional changes of the substituents influence the structure, redox behavior, and catalytic activity for NADH regeneration. Substitution at the 3,3' and 6,6' positions of the bpy ligand renders a greater electron density at the metal center and also gives the metallacycle a puckered shape due to the steric effect. An inverse relationship observed between the catalyst redox potential and activity was explained by the steric effect of the substituents and the kinetic studies of intermediate generation. The kinetic studies of intermediate generation provide valuable mechanistic insight into this catalytic cycle and future design strategy.

■ ASSOCIATED CONTENT

Supporting Information

The Supporting Information is available free of charge on the ACS Publications website at DOI: 10.1021/acs.inorgchem.6b02474.

Experimental details including the synthesis of rhodium complexes, ^1H NMR spectra, X-ray crystallographic information, UV–vis spectra, cyclic voltammograms, summary of characterization results table, kinetic studies of 1–5, and additional figures (PDF)

X-ray crystallographic files in CIF format of complex 2 (CIF)

X-ray crystallographic files in CIF format of complex 5 (CIF)

■ AUTHOR INFORMATION

Corresponding Author

*E-mail: yoona@kookmin.ac.kr.

ORCID

Sungho Yoon: 0000-0003-4521-2958

Notes

The authors declare no competing financial interest.

■ ACKNOWLEDGMENTS

We acknowledge financial support by a grant from the C1 Gas Refinery Program (Grant 2015M3D3A1A01064879) through

the National Research Foundation of Korea funded by the Ministry of Education, Science and Technology of Korean government and also from Global Scholarship Program for Foreign Graduate Students at Kookmin University, Korea.

REFERENCES

- (1) *Biocatalysis for the pharmaceutical industry: Discovery, Development, and Manufacturing*; Tao, J., Lin, G.-Q., Liese, A., Eds.; Wiley: Singapore, 2009.
- (2) *Biotechnology for clean industrial products and process: Towards Industrial Sustainability*; OECD: Paris, France, 1998.
- (3) van Beilen, J. B.; Duetz, W. A.; Schmid, A.; Witholt, B. Practical issues in the application of oxygenases. *Trends Biotechnol.* **2003**, *21* (4), 170–177.
- (4) Devaux-Basseguy, R.; Bergel, A.; Comtat, M. Potential applications of NAD(P)-dependent oxidoreductases in synthesis: A survey. *Enzyme Microb. Technol.* **1997**, *20* (4), 248–258.
- (5) Hummel, W. Large-scale applications of NAD(P)-dependent oxidoreductases: recent developments. *Trends Biotechnol.* **1999**, *17* (12), 487–492.
- (6) Straathof, A. J. J.; Panke, S.; Schmid, A. The production of fine chemicals by biotransformations. *Curr. Opin. Biotechnol.* **2002**, *13* (6), 548–556.
- (7) May, S. W.; Padgett, S. R. Oxidoreductase Enzymes in Biotechnology - Current Status and Future Potential. *Bio/Technology* **1983**, *1* (8), 677–686.
- (8) Xu, F. Applications of oxidoreductases: Recent progress. *Ind. Biotechnol.* **2005**, *1* (1), 38.
- (9) Chenault, H. K.; Whitesides, G. M. Regeneration of Nicotinamide Cofactors for Use in Organic-Synthesis. *Appl. Biochem. Biotechnol.* **1987**, *14* (2), 147–197.
- (10) Wu, H.; Tian, C.; Song, X.; Liu, C.; Yang, D.; Jiang, Z. Methods for the regeneration of nicotinamide coenzymes. *Green Chem.* **2013**, *15* (7), 1773–1789.
- (11) Hollmann, F.; Arends, I. W. C. E.; Buehler, K. Biocatalytic Redox Reactions for Organic Synthesis: Nonconventional Regeneration Methods. *ChemCatChem* **2010**, *2* (7), 762–782.
- (12) Quinto, T.; Kohler, V.; Ward, T. R. Recent Trends in Biomimetic NADH Regeneration. *Top. Catal.* **2014**, *57* (5), 321–331.
- (13) Schmid, A.; Dordick, J. S.; Hauer, B.; Kiener, A.; Wubbolts, M.; Witholt, B. Industrial biocatalysis today and tomorrow. *Nature* **2001**, *409* (6817), 258–268.
- (14) Betanzos-Lara, S.; Liu, Z.; Habtemariam, A.; Pizarro, A. M.; Qamar, B.; Sadler, P. J. Organometallic Ruthenium and Iridium Transfer-Hydrogenation Catalysts Using Coenzyme NADH as a Cofactor. *Angew. Chem., Int. Ed.* **2012**, *51* (16), 3897–3900.
- (15) Soldevila-Barreda, J. J.; Bruijninx, P. C. A.; Habtemariam, A.; Clarkson, G. J.; Deeth, R. J.; Sadler, P. J. Improved Catalytic Activity of Ruthenium-Arene Complexes in the Reduction of NAD⁺. *Organometallics* **2012**, *31* (16), 5958–5967.
- (16) Liu, Z.; Deeth, R. J.; Butler, J. S.; Habtemariam, A.; Newton, M. E.; Sadler, P. J. Reduction of Quinones by NADH Catalyzed by Organoiridium Complexes. *Angew. Chem., Int. Ed.* **2013**, *52* (15), 4194–4197.
- (17) Steckhan, E.; Herrmann, S.; Ruppert, R.; Dietz, E.; Frede, M.; Spika, E. Analytical Study of a Series of Substituted (2,2'-Bipyridyl)-(Pentamethylcyclopentadienyl) rhodium and iridium Complexes with Regard to Their Effectiveness as Redox Catalysts for the Indirect Electrochemical and Chemical Reduction of NAD(P)⁺. *Organometallics* **1991**, *10* (5), 1568–1577.
- (18) Lo, H. C.; Buriez, O.; Kerr, J. B.; Fish, R. H. Regioselective Reduction of NAD⁺ Models with [Cp*Rh(bpy)H]⁺: Structure-Activity Relationships and Mechanistic Aspects in the Formation of the 1,4-NADH Derivatives. *Angew. Chem., Int. Ed.* **1999**, *38* (10), 1429–1432.
- (19) Canivet, J.; Suss-Fink, G.; Stepnicka, P. Water-Soluble Phenanthroline Complexes of Rhodium, Iridium and Ruthenium for the Regeneration Of NADH in the Enzymatic Reduction of Ketones. *Eur. J. Inorg. Chem.* **2007**, *2007* (30), 4736–4742.
- (20) Sivanesan, D.; Yoon, S. Functionalized bipyridyl rhodium complex capable of electrode attachment for regeneration of NADH. *Polyhedron* **2013**, *57*, 52–56.
- (21) Hildebrand, F.; Kohlmann, C.; Franz, A.; Lutz, S. Synthesis, Characterization and Application of New Rhodium Complexes for Indirect Electrochemical Cofactor Regeneration. *Adv. Synth. Catal.* **2008**, *350* (6), 909–918.
- (22) Grau, M. M.; Poizat, M.; Arends, I. W. C. E.; Hollmann, F. Phosphite-driven, [Cp*Rh(bpy)(H₂O)]²⁺-catalyzed reduction of nicotinamide and flavin cofactors: characterization and application to promote chemoenzymatic reduction reactions. *Appl. Organomet. Chem.* **2010**, *24* (5), 380–385.
- (23) de Torres, M.; Dimroth, J.; Arends, I. W. C. E.; Keilitz, J.; Hollmann, F. Towards Recyclable NAD(P)H Regeneration Catalysts. *Molecules* **2012**, *17* (8), 9835–9841.
- (24) Maenaka, Y.; Suenobu, T.; Fukuzumi, S. Efficient Catalytic Interconversion between NADH and NAD⁺ Accompanied by Generation and Consumption of Hydrogen with a Water-Soluble Iridium Complex at Ambient Pressure and Temperature. *J. Am. Chem. Soc.* **2012**, *134* (1), 367–374.
- (25) Maenaka, Y.; Suenobu, T.; Fukuzumi, S. Hydrogen Evolution from Aliphatic Alcohols and 1,4-Selective Hydrogenation of NAD⁺ Catalyzed by a [C,N] and a [C,C] Cyclometalated Organoiridium Complex at Room Temperature in Water. *J. Am. Chem. Soc.* **2012**, *134* (22), 9417–9427.
- (26) Hollmann, F.; Kleeb, A.; Otto, K.; Schmid, A. Coupled chemoenzymatic transfer hydrogenation catalysis for enantioselective reduction and oxidation reactions. *Tetrahedron: Asymmetry* **2005**, *16*, 3512–3519.
- (27) Hollmann, F.; Witholt, B.; Schmid, A. [Cp*Rh(bpy)(H₂O)]²⁺: a versatile tool for efficient and non-enzymatic regeneration of nicotinamide and flavin coenzymes. *J. Mol. Catal. B: Enzym.* **2002**, *19-20*, 167–176.
- (28) Poizat, M.; Arends, I. W. C. E.; Hollmann, F. On the nature of mutual inactivation between [Cp*Rh(bpy)(H₂O)]²⁺ and enzymes - analysis and potential remedies. *J. Mol. Catal. B: Enzym.* **2010**, *63* (3–4), 149–156.
- (29) Kang, J. W.; Maitlis, P. M. The Conversion of Dewar Hexamethylbenzene to Pentamethylcyclopentadienylrhodium(III) Chloride. *J. Am. Chem. Soc.* **1968**, *90* (12), 3259–3261.
- (30) Sheldrick, G. M. A short history of SHELX. *Acta Crystallogr., Sect. A: Found. Crystallogr.* **2008**, *64*, 112–122.
- (31) Sheldrick, G. M. *SADABS: Area-Detector Absorption Correction*; University of Gottingen: Gottingen, Germany, 2001.
- (32) Spek, A. L. Structure validation in chemical crystallography. *Acta Crystallogr., Sect. D: Biol. Crystallogr.* **2009**, *65*, 148–155.
- (33) Newkome, G. R.; Patri, A. K.; Holder, E.; Schubert, U. S. Synthesis of 2,2'-Bipyridines: Versatile Building Blocks for Sexy Architectures and Functional Nanomaterials. *Eur. J. Org. Chem.* **2004**, *2004*, 235–254.
- (34) Dadci, L.; Elias, H.; Frey, U.; Hoernig, A.; Koelle, U.; Merbach, A. E.; Paulus, H.; Schneider, J. S. π -Arene Aqua Complexes of Cobalt, Rhodium, Iridium, and Ruthenium: Preparation, Structure, and Kinetics of Water Exchange and Water Substitution. *Inorg. Chem.* **1995**, *34* (1), 306–315.
- (35) Scharwitz, M. A.; Ott, I.; Geldmacher, Y.; Gust, R.; Sheldrick, W. S. Cytotoxic half-sandwich rhodium(III) complexes: Polypyridyl ligand influence on their DNA binding properties and cellular uptake. *J. Organomet. Chem.* **2008**, *693* (13), 2299–2309.
- (36) Youinou, M. T.; Ziesel, R. Synthesis and molecular structure of a new family of iridium(III) and rhodium(III) complexes: $[\eta^5\text{-Me}_5\text{C}_5\text{Ir}(\text{LL})\text{X}]^+$ and $[\eta^5\text{-Me}_5\text{C}_5\text{Rh}(\text{LL})\text{Cl}]^+$ - LL = 2,2'-bipyridine or 1,10-phenanthroline; X = Cl or H. Single crystal structures of $[\eta^5\text{-Me}_5\text{C}_5\text{Ir}(\text{bpy})\text{Cl}]\text{Cl}$ and $[\eta^5\text{-Me}_5\text{C}_5\text{Rh}(\text{Phen})\text{Cl}]\text{ClO}_4$. *J. Organomet. Chem.* **1989**, *363* (1–2), 197–208.
- (37) Ladwig, M.; Kaim, W. Spectroscopic and electrochemical properties of the isomeric bidiazine complexes $[(\text{C}_5\text{Me}_5)\text{ClRh}(\text{bdz})]^+$ and $(\text{C}_5\text{Me}_5)\text{Rh}(\text{bdz})$ and their relevance to the Catalysis of the 2

$H^+ \rightarrow H_2$ reaction by 2,2'-bipyridine analogs. *J. Organomet. Chem.* **1991**, 419 (1–2), 233–243.

(38) Kaim, W.; Reinhardt, R.; Sieger, M. Chemical and Electrochemical Generation of Hydride-Forming Catalytic Intermediates (bpy)M(CnRn): M = Rh, Ir (n = 5), M = Ru, Os (n = 6). Coordinatively Unsaturated Ground State Models of MLCT Excited States? *Inorg. Chem.* **1994**, 33 (20), 4453–4459.

(39) Ruppert, R.; Herrmann, S.; Steckhan, E. Very Efficient Reduction of NAD(P)⁺ with Formate Catalyzed by Cationic Rhodium Complexes. *J. Chem. Soc., Chem. Commun.* **1988**, 17, 1150–1151.

(40) Leiva, C.; Lo, H. C.; Fish, R. H. Aqueous organometallic chemistry. 3. Catalytic hydride transfer reactions with ketones and aldehydes using [Cp*Rh(bpy)(H₂O)](OTf)₂ as the precatalyst and sodium formate as the hydride source: Kinetic and activation parameters, and the significance of steric and electronic effects. *J. Organomet. Chem.* **2010**, 695 (2), 145–150.

(41) Pitman, C. L.; Finster, O. N. L.; Miller, A. J. M. Cyclopentadiene-mediated hydride transfer from rhodium complexes. *Chem. Commun.* **2016**, 52 (58), 9105–9108.

(42) Quintana, L. M. A.; Johnson, S. I.; Corona, S. L.; Villatoro, W.; Goddard, W. A.; Takase, M. K.; VanderVelde, D. G.; Winkler, J. R.; Gray, H. B.; Blakemore, J. D. Proton-hydride tautomerism in hydrogen evolution catalysis. *Proc. Natl. Acad. Sci. U. S. A.* **2016**, 113 (23), 6409–6414.

(43) Ito, M.; Kuwana, T. Spectroelectrochemical study of indirect reduction of triphosphopyridine nucleotide: I. Methyl viologen, ferredoxin-TPN-reductase and TPN. *J. Electroanal. Chem. Interfacial Electrochem.* **1971**, 32 (3), 415–425.

(44) Karyakin, A. A.; Ivanova, Y. N.; Karyakina, E. E. Equilibrium (NAD⁺/NADH) potential on poly(Neutral Red) modified electrode. *Electrochem. Commun.* **2003**, 5 (8), 677–680.

(45) Lo, H. C.; Leiva, C.; Buriez, O.; Kerr, J. B.; Olmstead, M. M.; Fish, R. H. Bioorganometallic chemistry. 13. Regioselective reduction of NAD⁺ models, 1-Benzylnicotinamide Triflate and β-Nicotinamide Ribose-5'-methyl Phosphate, with in Situ Generated [Cp*Rh(bpy)-H]⁺: Structure-Activity Relationships, Kinetics, and Mechanistic Aspects in the Formation of the 1,4-NADH Derivatives. *Inorg. Chem.* **2001**, 40 (26), 6705–6716.

(46) Steckhan, E.; Herrmann, S.; Ruppert, R.; Thommes, J.; Wandrey, C. Continuous Generation of NADH from NAD⁺ and Formate Using a Homogeneous Catalyst with Enhanced Molecular Weight in a Membrane Reactor. *Angew. Chem., Int. Ed. Engl.* **1990**, 29 (4), 388–390.

(47) Lutz, J.; Hollmann, F.; Ho, T. V.; Schnyder, A.; Fish, R. H.; Schmid, A. Bioorganometallic chemistry: biocatalytic oxidation reactions with biomimetic NAD⁺/NADH co-factors and [Cp*Rh-(bpy)H]⁺ for selective organic synthesis. *J. Organomet. Chem.* **2004**, 689 (25), 4783–4790.

(48) Ruppert, R.; Herrmann, S.; Steckhan, E. Efficient indirect electrochemical in-situ regeneration of nadh: electrochemically driven enzymatic reduction of pyruvate catalyzed by d-ldh. *Tetrahedron Lett.* **1987**, 28 (52), 6583–6586.

(49) Ogo, S.; Hayashi, H.; Uehara, K.; Fukuzumi, S. Crystallographic report: Crystal structures of organometallic aqua complexes [Cp*Rh^{III}(bpy)(OH₂)₂]²⁺ and [Cp*Rh^{III}(6,6'-Me₂bpy)(OH₂)₂]²⁺ used as key catalysts in regioselective reduction of NAD⁺ analogues. *Appl. Organomet. Chem.* **2005**, 19 (5), 639–643.

(50) Fukuzumi, S.; Kobayashi, T.; Suenobu, T. Efficient Catalytic Decomposition of Formic Acid for the Selective Generation of H₂ and H/D Exchange with a Water-Soluble Rhodium Complex in Aqueous Solution. *ChemSusChem* **2008**, 1 (10), 827–834.